Defect evolution of neutron irradiated ITER grade tungsten after annealing

D. Papadakis[1,2], K. Mergia[1,*] , E. Manios[1], V. Chatzikos[1,3], S. Dellis[1], D. Terentyev[4], G. Bonny[4], W. Van Renterghem[4], C.C. Chang[4,5] and S. Messoloras[1]

[1] *Institute of Nuclear and Radiological Sciences and Technology, Energy and Safety, NCSR Demokritos, Athens, 15310, Greece*
[2] *Department of Physics, School of Sciences, University of Athens, Athens, 15772, Greece*
[3] *Department of Physics, School of Sciences, University of Ioannina, Ioannina, 45110, Greece*
[4] *SCK CEN, Nuclear Materials Science Institute, Boeretang 200, 2400 Mol, Belgium*
[5] *Institute of Mechanics, Materials and Civil Engineering, UCLouvain, 1348 Louvain-la-Neuve, Belgium*

1 Abstract

The microstructural evolution of neutron irradiated tungsten (W) after annealing and its correlation with the corresponding mechanical properties provides valuable insight on the defect interactions and their annihilation processes. This would result in the identification of recovery mechanisms, leading to the design of healing processes and thus, enabling the lifetime extension of fusion reactor components. Within this framework, samples from ITER specification forged W bar were neutron irradiated to a dose of 0.2 displacements per atom (dpa) at 600 °C in the Belgian Material Test Reactor (BR2) and subsequently annealed at 800 and 1000 °C. The evolution of the irradiation induced defects after annealing has been assessed by transmission electron microscopy (TEM), positron annihilation lifetime spectroscopy and electrical resistivity and its effect on the mechanical properties are discussed in terms of Vickers hardness. Neutron irradiation results in the formation of dislocation loops and voids. TEM observations show an increase in the size of both defect types after post irradiation (PI) annealing at both temperatures, accompanied by an initial increase in their density after PI annealing at 800 °C, followed by a subsequent decrease after PI annealing at 1000 °C. The presence of TEM-irresolvable defects of both types is revealed in the as-irradiated state, which is evidenced by the evolution of Vickers hardness, resistivity and positron lifetimes and their correlation after the PI annealing. In the as-irradiated state, as well as after PI annealing at both temperatures, the hardening is dominated by voids.

Keywords: tungsten; post-irradiation annealing; TEM; positron annihilation spectroscopy; electrical resistivity; hardness

*Corresponding Author: Dr K. Mergia, email: kmergia@ipta.demokritos.gr

2 Introduction

Tungsten (W) is currently the baseline armour material for current and future fusion devices due to its numerous advantageous thermo-physical properties, low tritium retention, good sputtering resistance, low swelling, thermal stress and shock resistance, and high-temperature strength [1–6]. However, its low fracture toughness, low ductile-to-brittle transition temperature (DBTT) and low recrystallization temperature compared to the expected temperatures in a fusion device, impose limitations to its performance under service. Forged W bar is considered an ITER grade material to be used as a reference to other material options [3,7,8] with forging being one of the proposed methods of microstructural modification for decreasing DBTT down to room temperature and for improving its strength [3].

The response of W in a fusion environment is studied either through the use of ion irradiation [9–13], or through fission neutron irradiation [14–25] at high temperatures. Neutron irradiation damage leads to the creation of vacancy clusters or voids and dislocation loops [14–17,26,27] as well as transmutation products (namely Rhenium (Re), Osmium (Os) and Tantalum (Ta)[25]) which can also form precipitates [28] or clusters [18]. The specific type and population of defects are determined by the neutron irradiation conditions [19–24,28].

During fusion device operation with magnetically confined plasma, disruptions will locally cause an increase in temperature, further altering the microstructure, and thus the properties of the material. Therefore the study of the evolving microstructure of an as-irradiated material is of primary importance. Shedding light in the recovery stages of irradiated materials [29] could pave the way for implementing of on-site recovery annealing cycles, possibly allowing to extend the lifetime of the PFCs.

The evolution of defects after neutron or ion irradiation has been investigated in a number of works and the main findings can be summarized as follows: Stage III recovery regarding monovacancy migration can be identified in the range of 400 to 600 °C [11,17,30–35]. Above 650 and up to 900 °C stage IV recovery comprising of coalescence of small vacancy clusters [17,31,33–37] and dislocation loop growth and dislocation line rearrangement [11,17,31,32,37] occurs. Further annealing leads to complete defect recovery, which seems to be heavily dependent on the irradiation conditions, and is observed at 900 °C [33], 1300 °C [17],1500 °C [29,34,38] and 1700 °C [39].

In this work forged W bar, neutron irradiated to 0.2 displacements per atom (dpa) at 600 °C, has been annealed at 800 and 1000 °C. The evolution of the microstructure is investigated through transmission electron microscopy (TEM), electrical resistivity, positron annihilation lifetime spectroscopy (PALS) and Vickers hardness. The evolution of the microstructure at the two annealing temperatures and the correlation between microstructure and micromechanics is discussed.

3 Materials and Methods

3.1 Material, neutron irradiation and post-irradiation annealing

The W material in bar form was produced by PLANSEE SE in a powder metallurgical route consisting of sintering and hot forging from two orthogonal directions [40]. Samples were cut from the bar in disk form having a diameter of about 11 mm and a thickness of about 0.5 mm. The samples were irradiated in the BR2 reactor (for which the typical spectra can be found in [41]), at SCK CEN at 600 °C for a duration of 70 days to a neutron fluence of about 6×10^{20} n/cm^2 for E>0.1 MeV corresponding to a dose of 0.2 displacements per atom (dpa), as determined by MCNPX 2.7.0 calculations using a threshold displacement energy of 55 eV. The irradiation temperature was based on thermo-hydraulic calculations with estimated temperature fluctuations, due to neutron flux fluctuations and the burn out of the fuel element within a reactor cycle, of about 25 K. The samples were encapsulated in stainless steel tube filled with helium. The thickness (1.5 mm) of the steel tube was selected to maximize the shielding from the thermal neutrons and minimize the transmutation production. More details about the irradiation can be found in [42]. The Re, Os and Ta transmutation products have been evaluated by the FISPACT-II nuclide inventory code and employing TENDL-2019 nuclear library, for Re and Os, and EAF-2010 for Ta and they are found (0.54±0.06) at% Re, (0.013±0.002) at% Os and $(3.3\pm0.4)\times10^{-3}$ at% Ta. It is not noted that EAF-2010 was used for the evaluation of the W transmutation into Ta because there is a better agreement of the experimental activities determined by gamma spectroscopy measurements with the calculated ones for EAF-2010 nuclear library. The material studied through PALS, DC resistivity and Vickers hardness was post-irradiation (PI) annealed under high vacuum at the temperatures of 800 and 1000 °C for 24 hours at NCSR "Demokritos", while the one examined through TEM was PI annealed for 1 hour at SCK – CEN.

3.2 Methods

3.2.1 TEM

Transmission electron microscopy measurements were carried out using a JEOL 3010 TEM operating at 300 kV. The samples were prepared for TEM investigation by conventional electrochemical polishing method. Conventional bright field and dark field diffraction contrast images were recorded mostly under weak beam two beam conditions, while cavities were visualized in out-of-focus imaging conditions. Further information regarding the experimental setup and the method can be found in [43], where the original investigation is provided and results are discussed in detail.

3.2.2 PALS

Positron Annihilation Lifetime Spectroscopy measurements were carried out at room temperature, using the Ortec® PLS-system. A ^{22}Na radionuclide encapsulated in 3.6 mg/cm^2 thin polyimide (Kapton®) with an activity of 100 μCi was used as the positron source, sandwiched between two pieces of specimens. The detectors were placed in a linear configuration at a distance of about 3 mm from the sample. More details on the experimental setup and the analysis can be found in [44]. The data analysis was performed using LT10 software [45]. From the analysis of the data, the lifetime, τ_i, of each type i of defect and the probability, I_i, of the positron to be annihilated in type i defect ($\sum I_i = 1$) are determined.

3.2.3 DC Resistivity

Electrical resistivity was measured employing the collinear 4-point probe (4PP) method using Keithley 2182A nanovoltmeter and Keithley 6221 AC and DC source. In order to eliminate the thermoelectric voltage contribution in the measurements, the current source and the nanovoltometer are operated in tandem utilizing "Delta Mode". The measured resistance is converted to resistivity through a geometric factor, dependent on the sample's size [42].

3.2.4 Vickers hardness

Vickers depth-sensing indentation experiments were performed employing a NANOVEA's mechanical tester. The maximum load was set at 3 N, while both the loading and the unloading rate were 20 N/min. A dwell time of 200 s was applied before starting the unloading process. The loading rate was selected after a series of preliminary indentation tests to achieve stability in the hardness values. The holding time was chosen such as to attain equilibrium conditions, i.e. almost no change of the indentation depth. A set of six indentation tests, spaced by 200 µm, were performed for each measurement. An optical microscope was used to select the indented area free from visible defects.

4 Results and discussion

4.1 Microstructure evolution from TEM

The as-fabricated W material due to the forging process presents a dislocation line density of 4.5×10^{12} m^{-2}. Neutron irradiation at 600 °C results in the formation of dislocation loops and voids having densities and sizes as presented in Table I. Characteristic TEM images of the W forged bar sample after irradiation and PI annealing are presented in Figure 1. The figure contains two colums to illustrate separately the observation of voids (left one) and dislocation loops (right one). The dislocation loops appear as black dots and elliptical ripples in Figure 1b), 1d) and 1f), and the voids are depicted as white dots in Figure 1a), 1c) and 1e). The summary of the TEM characterization of the voids and loops is presented in Table I, in which the uncertainty reported regarding size is a measure of the width of the size distribution. TEM observations show an increase in the loop and void density and size after PI annealing at 800 °C. This indicates that a fraction of dislocation loops, too small to be resolved by TEM in the as-irradiated state, unpin and interact with each other, forming larger, TEM-resolvable loops. A similar effect is observed for the voids, with the increase in size indicating unpinning of vacancies or small vacancy clusters, leading to the formation of nano-sized voids through coalescence. In all cases, the smallest visible void size is about 0.8 nm, which is the instrument's resolution. Therefore the TEM observed increase in density after the annealing at 800 °C is due to the unpinning of TEM-invisible loops and self-interstitial atom clusters, and the TEM-determined density of the defects in the as-irradiated state is actually underestimated.

The increase in size, for both loops and voids, continues after annealing at 1000 °C. However, it is accompanied with a considerable decrease in the density of loops by about 53% and a small decrease in the density of voids by about 20%, compared to the corresponding values after PI annealing at 800 °C. These results suggest that some fraction of the loops has coalesced and some have been annihilated or removed by sinks such as dislocation lines and grain boundaries. For the voids, the reduction in density is associated with an increase in void volume fraction by 32%, hinting towards an Ostwald ripening process [46], i.e. growth of larger voids by the dissolution of smaller ones. An extended analysis of the TEM results can be found in [43].

A study involving the same material irradiated at a higher dose of 1 dpa at the same irradiation temperature and subsequently PI annealed at 800 °C for 1.5 h and 1000 °C for 1 h reported a similar trend of void microstructural evolution [37]. In the as irradiated state in [37], the increased dose by a factor of ~5 compared to that of the current study leads to an increased void density of the same factor. However, after PI annealing in [37] the corresponding increase in void density at both temperatures is only by a factor of ~2 higher compared to that of the current study. This indicates that higher damage doses result in a higher degree of recovery.

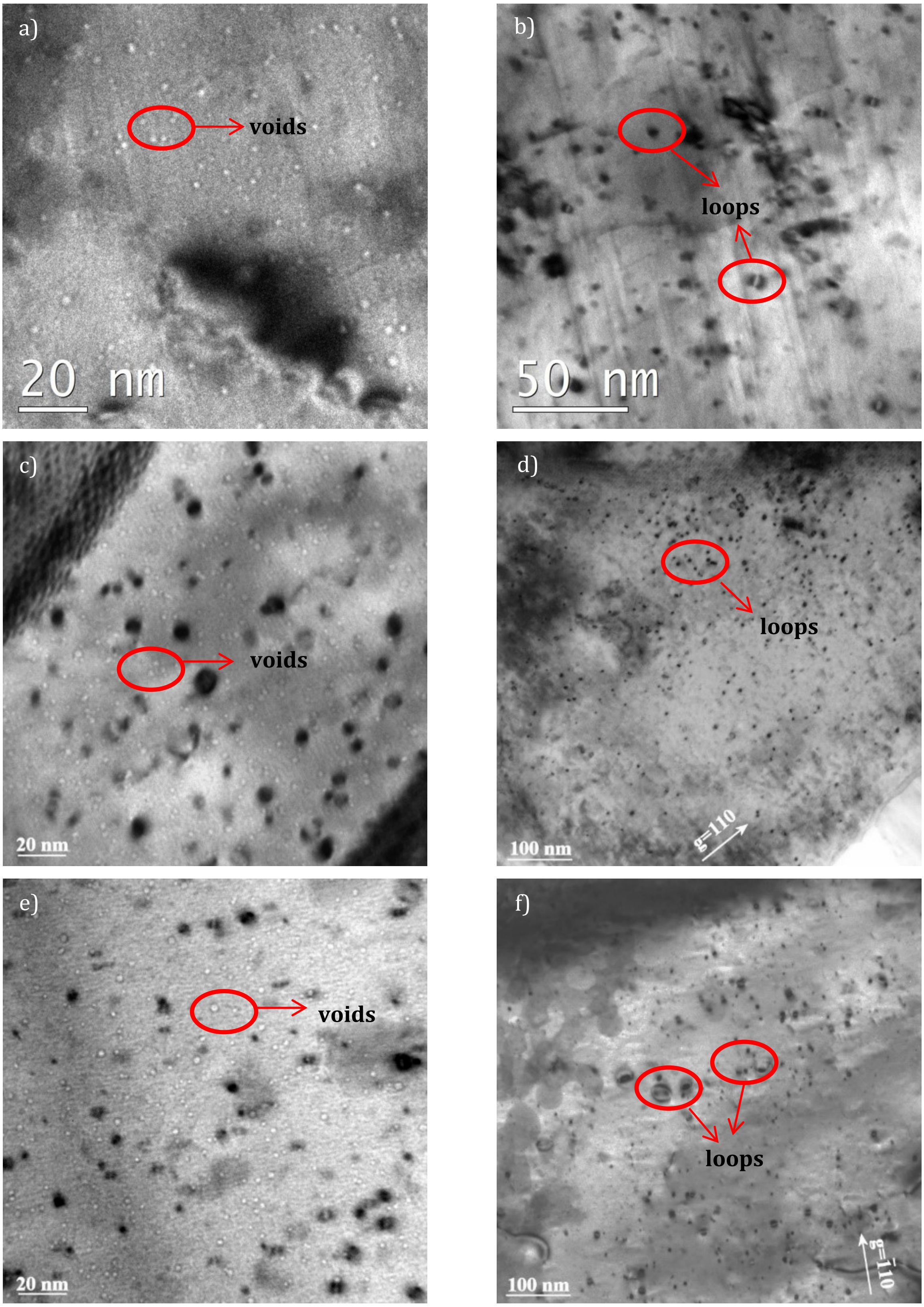

Figure 1: Under-focus bright field images showing the presence of voids in the as irradiated at 600 °C (a), PI annealed at 800 °C (c) and 1000 °C (e) forged W bar. Bright field images showing the presence of dislocation loops in the as-irradiated at 600 °C (b) and PI annealed at 800 °C (d) and 1000 °C (f) forged W bar.

Table I: Summary of the defect densities and sizes in the as-irradiated and PI annealed W forged bar as observed by TEM, along with the void length density determined from resistivity and hardness measurements (see section 4.4 for details).

	TEM							Hardness & Resistivity
	Loops			Voids				Voids
Sample condition	Density N_{loop} ($\times 10^{22}$ m^{-3})	Size d_{loop} (nm)	Linear density $\pi d_{loop} N_{loop}$ ($\times 10^{14}$ m^{-2})	Density N_{void} ($\times 10^{23}$ m^{-3})	Size d_{void} (nm)	Volume fraction (%)	Length Density $d_{void} \cdot N_{void}$ ($\times 10^{13}$ m^{-2})	Length Density $d_{void} \cdot N_{void}$ ($\times 10^{13}$ m^{-2})
As irrad. 0.2 dpa, 600 °C	2.3±0.3	2.8±1.7	2.0±1.2	0.4±0.3	1.4±0.5	0.006±0.008	6±5	16±2
PI annealed 800 °C	3.4±0.3	4.1±1.7	4.4±1.9	1.5±0.3	1.7±0.5	0.038±0.014	26±9	25±1
PI annealed 1000 °C	1.6±0.5	6.1±5.4	3.1±2.9	1.2±0.3	2.0±0.5	0.050±0.018	24±8	9±1

4.2 Open volume defects from PALS

From the analysis of the PALS spectra, two lifetimes were determined (Figure), a short one, τ_1 , and a long one, τ_2 .

In the unirradiated state, only the short lifetime, τ_1, can be identified, with a value of (152±1) ps. This lifetime is a compound time, considered as a weighted average of lifetimes for annihilations taking place in the defect-free bulk (100-110 ps) [10,47–52], in dislocations (130-180 ps) and possibly in mono-vacancies (160-200 ps) [10,17,32,47–52]. After irradiation τ_1 attains an increased value of (168±2) ps, indicative of the creation of irradiation induced dislocations in the material, which remains rather constant after PI annealing at 800 and 1000 °C having the values of (171±4) ps and (174±2) ps, respectively.

In the irradiated material the long lifetime τ_2 is found to be (498±5) ps. This value corresponds to the annihilation in vacancy clusters (containing more than 40 vacancies) or voids having a diameter larger than 1 nm. After PI annealing at 800 °C τ_2 increases to the value of (546±5) ps and to the value of (627±2) ps after PI annealing at 1000 °C, revealing an increase in void size at both temperatures. It is noted that theoretical calculations predict a small or no dependence of the positron lifetime on the void size due to the localization of the positron at the void surface, with a saturation positron lifetime value of around 500 ps [48,53]. Positron lifetimes larger than 500 ps and above the theoretical saturation value of 420 ps, are reported in proton [34] and neutron [17] post-irradiation annealed tungsten and they were attributed to pick-off annihilation of ortho-positronium formed in large vacancy clusters, suggesting that the internal surfaces of the clusters may be partially decorated with impurities [17]. The positron lifetime values for the voids found in the current study may be also related to the segregation of Re/Os at the void surface, which was evidenced by other experiments at a higher irradiation dose [54,55].

Regarding the relative intensities of the lifetime components, after irradiation and subsequent annealing, I_1 is around 60% and I_2 near 40%. The relative intensity is proportional to the trapping rate κ of the defect, which is equal to the defect number density, N, multiplied by the trapping strength, μ, of the defect, i.e. $I \propto \kappa = \mu N$. The fact that the intensities remain almost constant shows that the relative positron trapping rates of the two main types of defects – dislocations (lines and dislocation loops) and voids – do not significantly change after the PI annealing at 800 and 1000 °C. Taking into account that the number density of the voids decreases after the PI annealing, it may be inferred that the trapping strength of the voids increases as the their size increases after PI annealing.

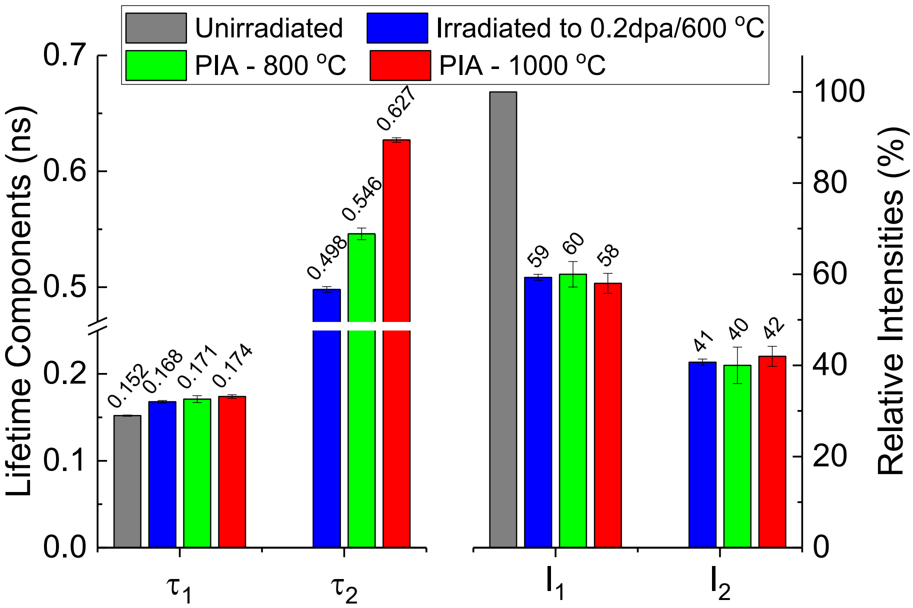

Figure 2: Positron annihilation lifetimes (left) and their relative intensities I_1 and I_2 (right) as determined by PALS, of the unirradiated, irradiated to 0.2 dpa at 600 °C and PI annealed at 800 and 1000 °C forged W bar.

4.3 DC Resistivity

DC resistivity measurements at room temperature were performed on the unirradiated, irradiated and PI annealed W, and the determined resistivity values are presented in Figure .

After irradiation an increase in resistivity by 24% is observed compared to the unirradiated sample, due to the creation of dislocations, voids and transmutation products in the material. Using the Matthiessen's rule [56] the radiation induced resistivity, RIR, which is the difference between the resistivity of the irradiated sample, ρ_{irrad}, and that of the unirradiated, $\rho_{unirrad}$, can be expressed as [57]

$$RIR \equiv \rho_{irrad} - \rho_{unirrad} = RIR_{void} + RIR_{disl} + RIR_{trans} \quad (1)$$

where RIR_{void}, RIR_{disl} and RIR_{trans} are the contributions of voids, dislocations (both loops and lines) and transmutation products to the radiation induced resistivity, respectively.

RIR_{void} can be estimated through the void diameter and number density as determined by TEM by using the specific resistivity of vacancies in tungsten [58–61]. This contribution is of the order of 10^{-2} μΩ·cm, and therefore can be ignored. The contribution of the transmutation products is calculated employing the specific resistivity for rhenium P_{Re} (~1.3 μΩ·cm/Re at.%) [62] and for osmium P_{Os} (~5 μΩ·cm/Os at.%) [63], and is found to be RIR_{trans} = (0.77 ± 0.08) μΩ·cm, assuming that Re and Os are homogeneously distributed in W matrix in solute form.

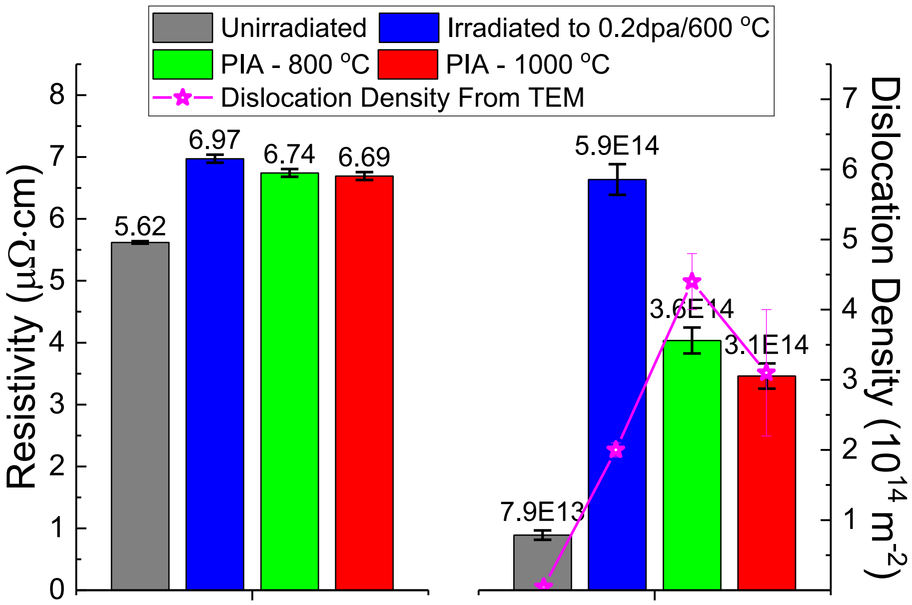

Figure 3: Measured DC resistivity (left) and the estimated dislocation densities (right) of the unirradiated, irradiated to 0.2 dpa at 600 °C and PI annealed at 800 and 1000 °C forged W bar. The TEM determined values of the dislocation densities from Table I are included for comparison.

For the contribution of dislocations in resistivity, the value for the dislocation specific resistivity, P_{DSR}, spans two orders of magnitude according to literature [64–67]. However, by utilizing the TEM measured dislocation density of the PI annealed W material at 1000 °C (Table I) and the resistivity from an unirradiated W bar material after complete recrystallization (ρ_{recr} = (5.54 ± 0.03) μΩ·cm), achieved after annealing at 1500 °C for 24 h [68], P_{DSR} can be obtained through the equation

$$\rho_{PIA-1000^{o}C} = \rho_{recr} + P_{DSR} \cdot N_{disl} + RIR_{trans} \quad (2)$$

since the recrystallized material W bar material contains the same impurity levels as the as – fabricated W bar, which affect resistivity. The choice of the PI annealed W material at 1000 °C is to minimize the percentage of loops that are unresolvable from TEM, as is the case of the as-irradiated state. The obtained value $P_{DSR} = 1\times10^{-23}\ \Omega\cdot\mathrm{m}^3$ is in good agreement with the previously determined value of $2.6\times10^{-23}\ \Omega\cdot\mathrm{m}^3$ in [42].

Utilizing the resistivity of the recrystallized forged W bar and eq. (1), the dislocation density can be determined for the unirradiated, the as-irradiated and the PI annealed at 800 °C and their values are presented in Figure .

The difference between the TEM determined value of the dislocation density and the one obtained from the resistivity measurement for the unirradiated (as fabricated) W material is attributed to the presence of dislocation loops created from the forging process [24], for which no exact numbers are provided by the TEM analysis due to their very low density (lower than 10^{20} m^{-3}) and large size variation. However, since the ones that were observed are usually larger than 50 nm in size, they could increase resistivity significantly. The discrepancy concerning the as-irradiated state is attributed to the underestimation of the loop dislocation density from TEM (as explained in section 3.2.1). The reduction in the resistivity after PI annealing to 800 °C is attributed mainly to dislocation line density reduction. However, it could be also due to a) agglomeration of a fraction of the transmutation products and to b) vacancy detrapping and migration, since vacancies and very small vacancy clusters may contribute significantly on the measured resistivity, however, when large vacancy clusters or voids are formed, this contribution diminishes. The subsequent recovery after the PI annealing at 1000 °C is attributed solely to the removal of dislocation loops.

4.4 Vickers Hardness

Vickers hardness measurements were performed on the unirradiated, irradiated and PI annealed forged W bar, and the determined Vickers hardness values are presented in Figure .

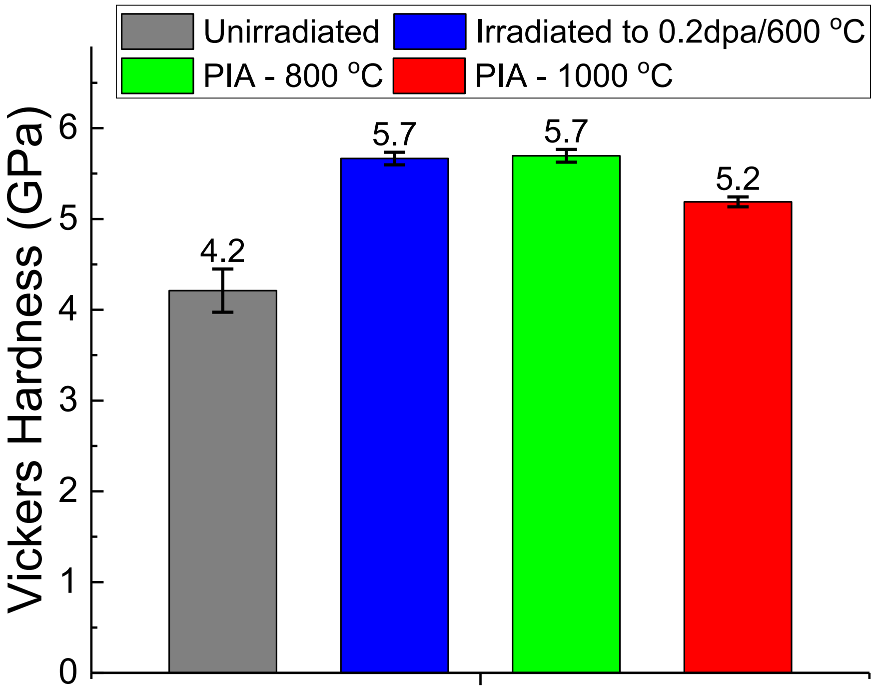

Figure 4: Vickers hardness of the unirradiated, irradiated to 0.2 dpa at 600 °C and PI annealed at 800 and 1000 °C forged W bar.

After irradiation of the material, a 36% increase in Vickers hardness is observed, due to the creation of dislocations and voids. After PI annealing at 800 °C the Vickers hardness remains unchanged, indicating that while the dislocation density is reduced (Figure) its effect in hardness is compensated by an increase in the density of nano-sized voids created from the possible unpinning of vacancies or small vacancy clusters and their coalescence. Further annealing at 1000 °C causes a 9% reduction in Vickers hardness, attributed to both nano-void coarsening and dislocation annihilation.

The increase in hardness after irradiation, RIH, can be associated with the radiation induced critical resolved shear stress (CRSS), $\Delta\tau_{CRSS}$, as

$$RIH \equiv H_{irrad} - H_{unirrad} = k\ \Delta\sigma = k\ M \Delta\tau_{CRSS} \tag{3}$$

where $H_{unirrad}$ and H_{irrad} the hardness of the unirradiated and as irradiated samples, respectively, $\Delta\sigma$ is the radiation induced yield strength [69], k is a factor of 3.2 for tungsten [70] and for M the value of 3.06 for non-textured BCC and FCC crystals [71] will be used. Using eq. (3) and the measured values of RIH the radiation induced critical resolved shear stress has been determined (Figure). In the same figure the contributions arising from dislocation and voids CRSS ($\Delta\tau_{disl}$ and τ_{voids}), as will be demonstrated below, are displayed.

Assuming that the lattice friction stress and the grain size do not change with irradiation and annealing, the induced CRSS arises from the radiation defects, i.e. dislocation loops and lines and voids, and it can be written according to the dispersed hardening barrier (DHB) model as [70,72]

$$\Delta\tau_{CRSS}^2 = \Delta\tau_{line}^2 + \Delta\tau_{loop}^2 + \tau_{void}^2 = G^2 b^2 \left(h_{line}^2 \Delta\rho_{line} + h_{loop}^2 \Delta\rho_{loop} + h_{void}^2 \rho_{void} \right) \tag{4}$$

where G is the shear modulus (159 GPa), b is the Burgers vector (0.274 nm), h_{line} is the dislocation line strength coefficient equal to 0.26 [73], h_{loop} has the value of 0.15 [17], h_{void} is the defect strength of voids which is dependent on their size [42], and in this case an average value of 0.2 will be used, and ρ is the defect length density ($\rho = N \cdot d$, N the defect number density and d the defect size). As the strength of dislocation lines and loops are very close and also the density of loops in the as-irradiated sample is 30 times larger than that of the lines eq. (4) can be approximated as

$$\Delta\tau_{CRSS}^2 = G^2 b^2 \left(h_{line}^2 \Delta\rho_{line} + h_{loop}^2 \Delta\rho_{loop} + h_{void}^2 \rho_{void} \right) \approx G^2 b^2 h_{loop}^2 \Delta\rho_{disl} + \tau_{void}^2 \tag{5}$$

where $\rho_{disl} = \rho_{loop} + \rho_{line}$. From the total dislocation line density determined by the electrical resistivity measurements (Figure) the radiation induced CRSS arising from all the dislocations (loops and lines), $\Delta\tau_{disl}$, can be determined, while the remaining contribution to the critical resolved shear stress is attributed to voids, as shown in Figure .

Examining the relative contributions of voids and dislocations to the total radiation induced critical resolved shear stress, it can be seen that the contribution of dislocations decreases rapidly after PI annealing at 800 °C. In every case, voids play the most important role in shaping the critical resolved shear stress of the material, with an almost complete dominance after PIA at 800 °C.

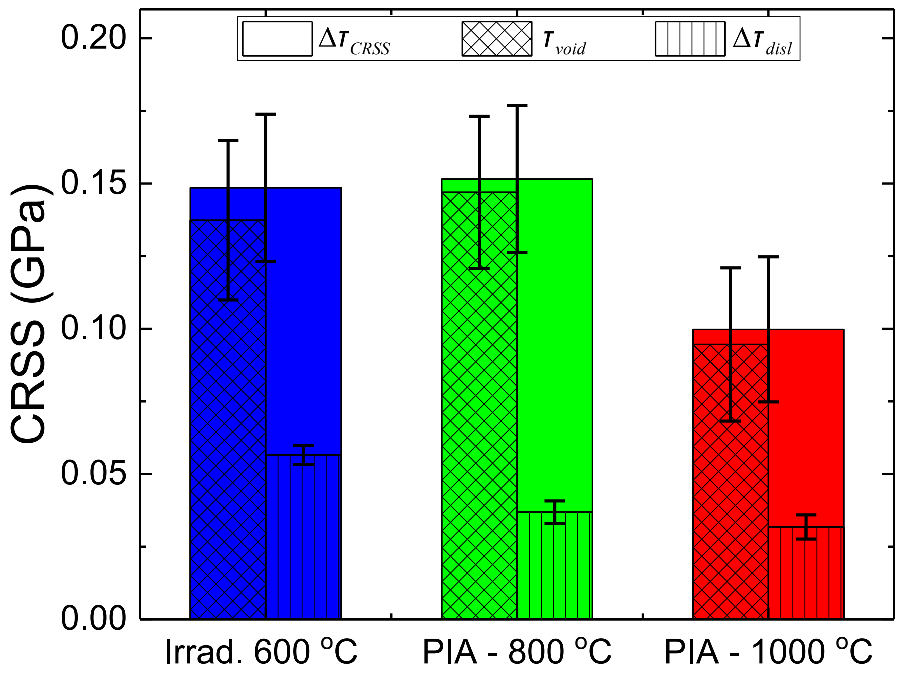

Figure 5: Irradiation induced critical resolved shear stress and the contribution from voids and dislocations, according to eq.3 and eq.4 for the unirradiated, irradiated to 0.2 dpa at 600 °C and PI annealed at 800 and 1000 °C forged W bar.

The CRSS arising from voids, τ_{void}, was utilized in order to calculate the void length density, $d_{void} \cdot N_{void}$, using eq.5, and its values are presented in Table I. It is observed that there is an excellent agreement between TEM data and the calculated values from hardness and resistivity after PI annealing at 800 °C. However, the determined value from resistivity and hardness results is three times higher in the as-irradiated state and three times lower after the PI annealing at 1000 °C. Regarding the as-irradiated state, this discrepancy confirms the reported remark in section 4.1 that TEM underestimates the density of defects in that state. For the discrepancy after the PI annealing at 1000 °C, the main reason lies in the annealing time difference between the TEM studied samples annealed for 1 hour and the samples studied by resistivity and hardness annealed for 24 h. Isothermal annealing at 1100 °C has shown that there is a significant hardness reduction between annealing for 1 and 24 h (results to be published), while the resistivity (mostly affected by dislocations) remains constant. This indicates that, regardless of the small temperature difference, the difference in annealing time could alter the final microstructure regarding voids significantly, explaining the observed discrepancy.

5 Summary and Conclusions

Tungsten in bar form, produced by PLANSEE SE in a powder metallurgical route consisting of sintering and hot forging was irradiated in the BR2 reactor, at SCK CEN, to 0.2 dpa at 600 °C and subsequently post irradiation (PI) annealed at 800 and 1000 °C. In order to probe the evolving microstructure TEM, PALS, resistivity and Vickers hardness measurements were performed after each post-irradiation annealing temperature.

Neutron irradiation to 0.2 dpa at 600 °C generates dislocation loops of 2.3×10^{22} m^{-3} density with an average diameter of 2.8 nm and voids of 4×10^{22} m^{-3} density with an average diameter of 1.4 nm, detectable directly from TEM and via their corresponding positron lifetimes from PALS. The presence of the irradiation induced defects increases the Vickers hardness and resistivity of the material by 36% and 24%, respectively.

TEM results, after PI annealing at 800 °C, show an increase in the defect sizes and densities, with the detection of dislocation loops of density $(3.4 \pm 0.3)\times10^{22}$ m^{-3} with an average diameter of (4.1 ± 1.7) nm and voids of density $(15 \pm 3)\times10^{22}$ m^{-3} with an average diameter of (1.7 ± 0.5) nm. The observed increase in density ~~is~~ arises from the fact that in the as-irradiated state there is a population of sub-nanometer defects that cannot be resolved by TEM. This is also inferred by the similar intensities of the positron annihilation lifetimes corresponding to dislocations and voids for the irradiated and PI annealed samples. This assertion is further supported by electrical resistivity measurements from which the total dislocation line density, from both dislocation loops and lines, after the neutron irradiation was determined and was found to be underestimated by TEM by a factor of three. A similar underestimation is revealed in the as-irradiated state of the material for the void length density (Table I) employing hardness values and the dispersed hardening barrier (DHB) model.

TEM and PALS show an increase in the void size after the PI annealing at both 800 and 1000 °C. This increase is accompanied by a slight decrease in their density of about 20% when the annealing temperature increases from 800 to 1000 °C. Regarding the dislocation loops their density decreases by about 53% as PI annealing increases from 800 to 1000 °C and their size shows a two-fold increase compared to the as-irradiated state and a 24% increase compared to PI annealing at 800 °C. A drop in the resistivity by about 3.3% after PI annealing at 800 °C is associated with the annihilation of dislocation loops. However, it is not followed by a change in hardness showing that while the dislocation loop density is reduced, its effect on the hardness is compensated by an increase in the density of nano-sized voids acting as strong obstacles. This may arise from the possible unpinning of vacancies or small vacancy clusters and their coalescence, thus contributing to the void density increase as well as void growth.

The trends of void and dislocation loop evolution with PI annealing reported above are in agreement with previous works in the literature. Specifically, in the temperature range of 800 °C to 1000 °C, the increase in size coupled with the decrease in density concerning voids [31,34,37,47] as well as dislocations [11,17,31,74] is within the range of a stage IV recovery process usually considered above 650 °C [74].

The above described evolution of the microstructure leads to a 9% decrease in hardness after PI annealing at 1000 °C. In the as-irradiated state as well as after PI annealing at both temperatures, voids dominate the hardening of the material, with their contribution peaking at 800 °C.

Acknowledgments

This work has been carried out within the framework of the EUROfusion Consortium and has received funding from the Euratom research and training programme 2014-2018, 2019-2020 and 2021-2025 under Grant Agreements Nos. 633053 and 101052200. The views and opinions expressed herein do not necessarily reflect those of the European Commission. The funding from the Hellenic General Secretariat for Research and Innovation for the Greek National Programme of the Controlled Thermonuclear Fusion is acknowledged.

References

[1] H. Bolt, V. Barabash, W. Krauss, J. Linke, R. Neu, S. Suzuki, N. Yoshida, Materials for the plasma-facing components of fusion reactors, J. Nucl. Mater. 329–333 (2004) 66–73. https://doi.org/10.1016/j.jnucmat.2004.04.005.

[2] R.A. Pitts, S. Carpentier, F. Escourbiac, T. Hirai, V. Komarov, S. Lisgo, A.S. Kukushkin, A. Loarte, M. Merola, A. Sashala Naik, R. Mitteau, M. Sugihara, B. Bazylev, P.C. Stangeby, A full tungsten divertor for ITER: Physics issues and design status, J. Nucl. Mater. 438 (2013) S48--S56. https://doi.org/10.1016/j.jnucmat.2013.01.008.

[3] G. Pintsuk, Tungsten as a Plasma-Facing Material, in: Compr. Nucl. Mater., Elsevier, Amsterdam, The Netherlands, 2012: pp. 551–581. https://doi.org/10.1016/B978-0-08-056033-5.00118-X.

[4] J.W. Davis, V.R. Barabash, A. Makhankov, L. Plöchl, K.T. Slattery, Assessment of tungsten for use in the ITER plasma facing components, J. Nucl. Mater. 258–263 (1998) 308–312. https://doi.org/10.1016/S0022-3115(98)00285-2.

[5] V. Philipps, Tungsten as material for plasma-facing components in fusion devices, J. Nucl. Mater. 415 (2011) S2--S9. https://doi.org/10.1016/j.jnucmat.2011.01.110.

[6] J.H. Yu, H. Tanigawa, D. Hamaguchi, T. Nozawa, Mechanical properties of three kinds of ITER-Grade pure tungsten with different manufacturing processes, Fusion Eng. Des. 157 (2020) 111679. https://doi.org/10.1016/j.fusengdes.2020.111679.

[7] O. Motojima, The ITER project construction status, Nucl. Fusion. 55 (2015) 104023. https://doi.org/10.1088/0029-5515/55/10/104023.

[8] C. Yin, D. Terentyev, T. Pardoen, A. Bakaeva, R. Petrov, S. Antusch, M. Rieth, M. Vilémová, J. Matějíček, T. Zhang, Tensile properties of baseline and advanced tungsten grades for fusion applications, Int. J. Refract. Met. Hard Mater. 75 (2018) 153–162. https://doi.org/10.1016/j.ijrmhm.2018.04.003.

[9] B. Wielunska, T. Płociński, T. Schwarz-Selinger, M. Mayer, W. Jacob, L. Ciupiński, Dislocation structure of tungsten irradiated by medium to high-mass ions, Nucl. Fusion. 62 (2022) 096003. https://doi.org/10.1088/1741-4326/ac75ff.

[10] C.L. Dube, P.K. Kulriya, D. Dutta, P.K. Pujari, Y. Patil, M. Mehta, P. Patel, S.S. Khirwadkar, Positron annihilation lifetime measurement and X-ray analysis on 120 MeV Au+7 irradiated polycrystalline tungsten, J. Nucl. Mater. 467 (2015) 406–412. https://doi.org/10.1016/j.jnucmat.2015.05.029.

[11] J. Grzonka, Ł. Ciupiński, J. Smalc-Koziorowska, O.V. Ogorodnikova, M. Mayer, K.J. Kurzydłowski, Electron microscopy observations of radiation damage in irradiated and annealed tungsten, Nucl. Instruments Methods Phys. Res. Sect. B Beam Interact. with Mater. Atoms. 340 (2014) 27–33. https://doi.org/10.1016/j.nimb.2014.07.043.

[12] X. Yi, M.L. Jenkins, M.A. Kirk, Z. Zhou, S.G. Roberts, In-situ TEM studies of 150 keV W+ ion irradiated W and W-alloys: Damage production and microstructural evolution, Acta Mater. 112 (2016) 105–120. https://doi.org/10.1016/j.actamat.2016.03.051.

[13] X. Yi, M.L. Jenkins, M. Briceno, S.G. Roberts, Z. Zhou, M.A. Kirk, In situ study of self-ion irradiation damage in W and W-5Re at 500°C, Philos. Mag. 93 (2013) 1715–1738.

https://doi.org/10.1080/14786435.2012.754110.

[14] R.C. Rau, R.L. Ladd, J. Moteff, Voids in irradiated tungsten and molybdenum, J. Nucl. Mater. 33 (1969) 324–327. https://doi.org/10.1016/0022-3115(69)90029-4.

[15] J.T. Buswell, Vacancy damage in heavy ion and neutron-irradiated tungsten, Philos. Mag. 22 (1970) 787–802. https://doi.org/10.1080/14786437008220947.

[16] O. V. Ogorodnikova, M. Majerle, J. Čížek, S. Simakov, V. V. Gann, P. Hruška, J. Kameník, J. Pospíšil, M. Štefánik, M. Vinš, Positron annihilation spectroscopy study of radiation-induced defects in W and Fe irradiated with neutrons with different spectra, Sci. Rep. 10 (2020) 1–13. https://doi.org/10.1038/s41598-020-75737-8.

[17] X. Hu, T. Koyanagi, M. Fukuda, Y. Katoh, L.L. Snead, B.D. Wirth, Defect evolution in single crystalline tungsten following low temperature and low dose neutron irradiation, J. Nucl. Mater. 470 (2016) 278–289. https://doi.org/10.1016/j.jnucmat.2015.12.040.

[18] M.J. Lloyd, R.G. Abernethy, M.R. Gilbert, I. Griffiths, P.A.J.J. Bagot, D. Nguyen-Manh, M.P. Moody, D.E.J.J. Armstrong, Decoration of voids with rhenium and osmium transmutation products in neutron irradiated single crystal tungsten, Scr. Mater. 173 (2019) 96–100. https://doi.org/10.1016/j.scriptamat.2019.07.036.

[19] A. Hasegawa, M. Fukuda, K. Yabuuchi, S. Nogami, Neutron irradiation effects on the microstructural development of tungsten and tungsten alloys, J. Nucl. Mater. 471 (2016) 175–183. https://doi.org/10.1016/j.jnucmat.2015.10.047.

[20] V.K. Sikka, J. Moteff, Superlattice of voids in neutron-irradiated tungsten, J. Appl. Phys. 43 (1972) 4942–4944. https://doi.org/10.1063/1.1661050.

[21] M. Fukuda, K. Yabuuchi, S. Nogami, A. Hasegawa, T. Tanaka, Microstructural development of tungsten and tungsten-rhenium alloys due to neutron irradiation in HFIR, J. Nucl. Mater. 455 (2014) 460–463. https://doi.org/10.1016/j.jnucmat.2014.08.002.

[22] M. Fujitsuka, B. Tsuchiya, I. Mutoh, T. Tanabe, T. Shikama, Effect of neutron irradiation on thermal diffusivity of tungsten–rhenium alloys, J. Nucl. Mater. 283–287 (2000) 1148–1151. https://doi.org/10.1016/S0022-3115(00)00170-7.

[23] L.M.M. Garrison, Y. Katoh, N.A.P.K.A.P.K. Kumar, Mechanical properties of single-crystal tungsten irradiated in a mixed spectrum fission reactor, J. Nucl. Mater. 518 (2019) 208–225. https://doi.org/10.1016/j.jnucmat.2019.02.050.

[24] A. Dubinko, D. Terentyev, C. Yin, W. Van Renterghem, B. Rossaert, M. Rieth, E.E.E. Zhurkin, A. Zinovev, C.C.C. Chang, S. Van Dyck, G. Bonny, Microstructure and hardening induced by neutron irradiation in single crystal, ITER specification and cold rolled tungsten, Int. J. Refract. Met. Hard Mater. 98 (2021) 105522. https://doi.org/10.1016/j.ijrmhm.2021.105522.

[25] M.R.R. Gilbert, J.-C. Sublet, Neutron-induced transmutation effects in W and W-alloys in a fusion environment, Nucl. Fusion. 51 (2011) 43005. https://doi.org/10.1088/0029-5515/51/4/043005.

[26] M. Rieth, S.L. Dudarev, S.M. Gonzalez De Vicente, J. Aktaa, T. Ahlgren, S. Antusch, D.E.J. Armstrong, M. Balden, N. Baluc, M.F. Barthe, W.W. Basuki, M. Battabyal, C.S. Becquart, D. Blagoeva, H. Boldyryeva, J. Brinkmann, M. Celino, L. Ciupinski, J.B. Correia, A. De Backer, C. Domain, E. Gaganidze, C. García-Rosales, J. Gibson, M.R. Gilbert, S. Giusepponi, B. Gludovatz, H. Greuner, K. Heinola, T. Höschen, A. Hoffmann, N. Holstein, F. Koch, W. Krauss, H. Li, S.

Lindig, J. Linke, C. Linsmeier, P. López-Ruiz, H. Maier, J. Matejicek, T.P. Mishra, M. Muhammed, A. Muñoz, M. Muzyk, K. Nordlund, D. Nguyen-Manh, J. Opschoor, N. Ordás, T. Palacios, G. Pintsuk, R. Pippan, J. Reiser, J. Riesch, S.G. Roberts, L. Romaner, M. Rosiński, M. Sanchez, W. Schulmeyer, H. Traxler, A. Ureña, J.G. Van Der Laan, L. Veleva, S. Wahlberg, M. Walter, T. Weber, T. Weitkamp, S. Wurster, M.A. Yar, J.H. You, A. Zivelonghi, Recent progress in research on tungsten materials for nuclear fusion applications in Europe, J. Nucl. Mater. 432 (2013) 482–500. https://doi.org/10.1016/j.jnucmat.2012.08.018.

[27] J.A. Brinkman, On the Nature of Radiation Damage in Metals, J. Appl. Phys. 25 (1954) 961–970. https://doi.org/10.1063/1.1721810.

[28] M. Klimenkov, U. Jäntsch, M. Rieth, H.C.C. Schneider, D.E.J.E.J. Armstrong, J. Gibson, S.G.G. Roberts, Effect of neutron irradiation on the microstructure of tungsten, Nucl. Mater. Energy. 9 (2016) 480–483. https://doi.org/10.1016/j.nme.2016.09.010.

[29] D. Papadakis, K. Mergia, E. Manios, V. Chatzikos, S. Dellis, S. Messoloras, Post neutron irradiation annealing and defect evolution in single crystal tungsten, Nucl. Mater. Energy. 34 (2023) 101357. https://doi.org/10.1016/j.nme.2022.101357.

[30] P.E. Lhuillier, M.F. Barthe, P. Desgardin, W. Egger, P. Sperr, Positron annihilation studies on the nature and thermal behaviour of irradiation induced defects in tungsten, Phys. Status Solidi. 6 (2009) 2329–2332. https://doi.org/10.1002/pssc.200982114.

[31] B. Horvath, Y. Dai, Y. Lee, Annealing effect on the microstructure of tungsten irradiated in SINQ target, J. Nucl. Mater. 506 (2018) 19–25. https://doi.org/10.1016/J.JNUCMAT.2017.12.020.

[32] P.M.G.G. Nambissan, P. Sen, Positron annihilation study of the annealing behaviour of alpha induced defects in tungsten, Radiat. Eff. Defects Solids. 124 (1992) 215–221. https://doi.org/10.1080/10420159208220193.

[33] O.V. Ogorodnikova, L.Y. Dubov, S.V. Stepanov, D. Terentyev, Y.V. Funtikov, Y.V. Shtotsky, V.S. Stolbunov, V. Efimov, K. Gutorov, Annealing of radiation-induced defects in tungsten: Positron annihilation spectroscopy study, J. Nucl. Mater. 517 (2019) 148–151. https://doi.org/10.1016/j.jnucmat.2019.02.010.

[34] M. Zibrov, W. Egger, J. Heikinheimo, M. Mayer, F. Tuomisto, Vacancy cluster growth and thermal recovery in hydrogen-irradiated tungsten, J. Nucl. Mater. 531 (2020) 152017. https://doi.org/10.1016/j.jnucmat.2020.152017.

[35] O.V. Ogorodnikova, Y. Gasparyan, V. Efimov, Ł. Ciupiński, J. Grzonka, Annealing of radiation-induced damage in tungsten under and after irradiation with 20MeV self-ions, J. Nucl. Mater. 451 (2014) 379–386. https://doi.org/10.1016/j.jnucmat.2014.04.011.

[36] D. Papadakis, K. Mergia, S. Dellis, E. Manios, D. Terentyev, G. Bonny, A. Dubinko, W. Van Renterghem, M.J. Konstantinović, S. Messoloras, Post neutron irradiation annealing and defect evolution in tungsten single crystal, Nucl. Mater. Energy. (n.d.).

[37] A. Chauhan, Q. Yuan, D. Litvinov, E. Gaganidze, H.C. Schneider, D. Terentyev, J. Aktaa, Effect of temperature on the neutron irradiation-induced cavities in tungsten, Philos. Mag. 102 (2022) 1665–1683. https://doi.org/10.1080/14786435.2022.2079750.

[38] M.I. Zakharova, N.A. Artemov, V. V. Bogdanov, Effects of neutron irradiation and annealing on the elastic moduli and electrical resistivity of molybdenum and tungsten single crystals,

Inorg. Mater. 37 (2001) 786–789. https://doi.org/10.1023/A:1017979230262.

[39] M. Zibrov, T. Dürbeck, W. Egger, M. Mayer, High temperature recovery of radiation defects in tungsten and its effect on deuterium retention, Nucl. Mater. Energy. 23 (2020) 100747. https://doi.org/10.1016/j.nme.2020.100747.

[40] S. Krimpalis, K. Mergia, S. Messoloras, A. Dubinko, D. Terentyev, K. Triantou, J. Reiser, G. Pintsuk, Comparative study of the mechanical properties of different tungsten materials for fusion applications, Phys. Scr. T170 (2017) 014068. https://doi.org/10.1088/1402-4896/aa9292.

[41] J.C. Sublet, I.P. Bondarenko, G. Bonny, J.L. Conlin, M.R. Gilbert, L.R. Greenwood, P.J. Griffin, P. Helgesson, Y. Iwamoto, V.A. Khryachkov, T.A. Khromyleva, A.Y. Konobeyev, N. Lazarev, L. Luneville, F. Mota, C.J. Ortiz, D. Rochman, S.P. Simakov, D. Simeone, H. Sjostrand, D. Terentyev, R. Vila, Neutron-induced damage simulations: Beyond defect production cross-section, displacement per atom and iron-based metrics, Eur. Phys. J. Plus. 134 (2019) 350. https://doi.org/10.1140/epjp/i2019-12758-y.

[42] K. Mergia, V. Chatzikos, E. Manios, S. Dellis, D. Papadakis, D. Terentyev, G. Bonny, A. Dubinko, I.E. Stamatelatos, S. Messoloras, M. Rieth, Evolution of microstructure in neutron irradiated cold rolled tungsten and its correlation with hardness, Fusion Eng. Des. 172 (2021) 112784. https://doi.org/10.1016/j.fusengdes.2021.112784.

[43] W. Van Renterghem, G. Bonny, D. Terentyev, TEM investigation of neutron irradiated and post irradiation annealed tungsten materials, Fusion Eng. Des. 180 (2022) 113170. https://doi.org/10.1016/j.fusengdes.2022.113170.

[44] V. Chatzikos, K. Mergia, G. Bonny, D. Terentyev, D. Papadakis, G.E. Pavlou, S. Messoloras, Positron annihilation spectroscopy investigation of defects in neutron irradiated tungsten materials, Int. J. Refract. Met. Hard Mater. 105 (2022) 105838. https://doi.org/10.1016/j.ijrmhm.2022.105838.

[45] D. Giebel, J. Kansy, LT10 Program for Solving Basic Problems Connected with Defect Detection, Phys. Procedia. 35 (2012) 122–127. https://doi.org/10.1016/j.phpro.2012.06.022.

[46] A.D. Brailsford, R. Bullough, The rate theory of swelling due to void growth in irradiated metals, J. Nucl. Mater. 44 (1972) 121–135. https://doi.org/10.1016/0022-3115(72)90091-8.

[47] V.S. Subrahmanyam, P.M.G. Nambissan, P. Sen, Helium bubbles in tungsten studied by positron annihilation, Solid State Commun. 89 (1994) 523–527. https://doi.org/10.1016/0038-1098(94)90749-8.

[48] T. Troev, E. Popov, N. Nankov, T. Yoshiie, Model calculation of positron states in tungsten containing hydrogen and helium, J. Phys. Conf. Ser. 207 (2010) 12033. https://doi.org/10.1088/1742-6596/207/1/012033.

[49] S. Zhu, Y. Xu, Z. Wang, Y. Zheng, D. Zhou, E. Du, D. Yuan, M. Fukuda, M. Mihara, K. Matsuta, T. Minamisono, Positron annihilation lifetime spectroscopy on heavy ion irradiated stainless steels and tungsten, J. Nucl. Mater. 343 (2005) 330–332. https://doi.org/10.1016/j.jnucmat.2004.11.024.

[50] J. De Vries, Positron Lifetime Technique with Applications in Material Science, 1987.

[51] J. Heikinheimo, K. Mizohata, J. Räisänen, T. Ahlgren, P. Jalkanen, A. Lahtinen, N. Catarino, E. Alves, F. Tuomisto, Direct observation of mono-vacancy and self-interstitial recovery in

tungsten, APL Mater. 7 (2019) 21103. https://doi.org/10.1063/1.5082150.

[52] A. Yabuuchi, M. Tanaka, A. Kinomura, Short positron lifetime at vacancies observed in electron-irradiated tungsten: Experiments and first-principles calculations, J. Nucl. Mater. 542 (2020) 152473. https://doi.org/10.1016/j.jnucmat.2020.152473.

[53] M. Eldrup, B.N.N. Singh, Studies of defects and defect agglomerates by positron annihilation spectroscopy, J. Nucl. Mater. 251 (1997) 132–138. https://doi.org/10.1016/S0022-3115(97)00221-3.

[54] M. Klimenkov, M. Dürrschnabel, U. Jäntsch, P. Lied, M. Rieth, H.C. Schneider, D. Terentyev, W. Van Renterghem, Microstructural analysis of W irradiated at different temperatures, J. Nucl. Mater. 572 (2022) 154018. https://doi.org/10.1016/j.jnucmat.2022.154018.

[55] M. Dürrschnabel, M. Klimenkov, U. Jäntsch, M. Rieth, H.C. Schneider, D. Terentyev, New insights into microstructure of neutron-irradiated tungsten, Sci. Rep. 11 (2021) 1–17. https://doi.org/10.1038/s41598-021-86746-6.

[56] P.L. Rossiter, The electrical resistivity of metals and alloys, Electr. Resist. Met. Alloy. (1987). https://doi.org/10.1017/cbo9780511600289.

[57] D. Papadakis, S. Dellis, V. Chatzikos, E. Manios, I.E. Stamatelatos, S. Messoloras, K. Mergia, Neutron irradiation effects in different tungsten microstructures, Phys. Scr. 96 (2021) 124041. https://doi.org/10.1088/1402-4896/ac1eb2.

[58] J.W. Martin, R. Paetsch, Electrical resistivity of voids, J. Phys. F Met. Phys. 3 (1973) 907–917. https://doi.org/10.1088/0305-4608/3/5/005.

[59] J.W. Martin, The electrical resistivity due to structural defects, Philos. Mag. 24 (1971) 555–566. https://doi.org/10.1080/14786437108217029.

[60] J.W. Martin, The electrical resistivity of some lattice defects in FCC metals observed in radiation damage experiments, J. Phys. F Met. Phys. 2 (1972) 842–853. https://doi.org/10.1088/0305-4608/2/5/008.

[61] K.-D.D. Rasch, R.W. Siegel, H. Schultz, Quenching and recovery investigations of vacancies in tungsten, Philos. Mag. A. 41 (1980) 91–117. https://doi.org/10.1080/01418618008241833.

[62] L. Uray, P. Tekula-Buxbaum, Resistivity contribution of solutes in tungsten, J. Less Common Met. 123 (1986) 95–100. https://doi.org/10.1016/0022-5088(86)90119-0.

[63] T. Tanno, A. Hasegawa, M. Fujiwara, J.C. He, S. Nogami, M. Satou, T. Shishido, K. Abe, Precipitation of solid transmutation elements in irradiated tungsten alloys, Mater. Trans. 49 (2008) 2259–2264. https://doi.org/10.2320/matertrans.MAW200821.

[64] Z.S. Basinski, J.S. Dugdale, A. Howie, The electrical resistivity of dislocations, Philos. Mag. 8 (1963) 1989–1997. https://doi.org/10.1080/14786436308209092.

[65] H.B. Shukovsky, R.M. Rose, J. Wulff, The low temperature electrical resistivity of lattice defects in deformed tungsten single crystals, Acta Metall. 14 (1966) 821–830. https://doi.org/10.1016/0001-6160(66)90002-2.

[66] R.A. Brown, Electrical resistivity of dislocations in metals, J. Phys. F Met. Phys. 7 (1977) 1283–1295. https://doi.org/10.1088/0305-4608/7/7/026.

[67] A.S. Karolik, A.A. Luhvich, Calculation of electrical resistivity produced by dislocations and grain boundaries in metals, J. Phys. Condens. Matter. 6 (1994) 873–886. https://doi.org/10.1088/0953-8984/6/4/007.

[68] L. Tanure, A. Bakaeva, A. Dubinko, D. Terentyev, K. Verbeken, Effect of annealing on microstructure, texture and hardness of ITER-specification tungsten analyzed by EBSD, vickers micro-hardness and nano-indentation techniques, J. Nucl. Mater. 524 (2019) 191–199. https://doi.org/10.1016/j.jnucmat.2019.07.005.

[69] D. Tabor, The physical meaning of indentation and scratch hardness, Br. J. Appl. Phys. 7 (1956) 159–166. https://doi.org/10.1088/0508-3443/7/5/301.

[70] X. Hu, T. Koyanagi, M. Fukuda, N.A.P.K. Kumar, L.L. Snead, B.D. Wirth, Y. Katoh, Irradiation hardening of pure tungsten exposed to neutron irradiation, J. Nucl. Mater. 480 (2016) 235–243. https://doi.org/10.1016/j.jnucmat.2016.08.024.

[71] R.E.E. Stoller, S.J.J. Zinkle, On the relationship between uniaxial yield strength and resolved shear stress in polycrystalline materials, J. Nucl. Mater. 283–287 (2000) 349–352. https://doi.org/10.1016/S0022-3115(00)00378-0.

[72] S.. J. Zinkle, Y. Matsukawa, Observation and analysis of defect cluster production and interactions with dislocations, J. Nucl. Mater. 329–333 (2004) 88–96. https://doi.org/10.1016/j.jnucmat.2004.04.298.

[73] D. Terentyev, X. Xiao, A. Dubinko, A. Bakaeva, H. Duan, Dislocation-mediated strain hardening in tungsten: Thermo-mechanical plasticity theory and experimental validation, J. Mech. Phys. Solids. 85 (2015) 1–15. https://doi.org/10.1016/j.jmps.2015.08.015.

[74] F. Ferroni, X. Yi, K. Arakawa, S.P. Fitzgerald, P.D. Edmondson, S.G. Roberts, High temperature annealing of ion irradiated tungsten, Acta Mater. 90 (2015) 380–393. https://doi.org/10.1016/j.actamat.2015.01.067.